Published in final edited form as:
Cell. 2009 December 11; 139(6): 1157–1169. doi:10.1016/j.cell.2009.11.014.

Reduced IGF-1 Signaling Delays Age-associated Proteotoxicity in Mice

Ehud Cohen[1,*], **Johan F. Paulsson**[2], **Pablo Blinder**[3], **Tal Burstyn-Cohen**[4], **Deguo Du**[2], **Gabriela Estepa**[1], **Anthony Adame**[5], **Hang M. Pham**[5], **Martin Holzenberger**[6], **Jeffery W. Kelly**[2], **Eliezer Masliah**[5], and **Andrew Dillin**[1,§]

[1]Howard Hughes Medical Institute, Glenn Center for Aging Research, Molecular and Cell Biology Laboratory, The Salk Institute for Biological Studies, 10010 N. Torrey Pines Road, La Jolla, CA 92037, USA

[2]Department of Chemistry and Molecular and Experimental Medicine and The Skaggs Institute of Chemical Biology, The Scripps Research Institute, 10550 N. Torrey Pines Road, La Jolla, CA 92037, USA

[3]Department of Physics, University of California San Diego

[4]Molecular Neurobiology Laboratory, The Salk Institute for Biological Studies, 10010 N. Torrey Pines Road, La Jolla, CA 92037, USA

[5]Department of Neurosciences, University of California San Diego, 9500 Gilman Drive, La Jolla, CA 92093, USA

[6]INSERM 938, Hôpital Saint-Antoine, Paris, France

Summary

The Insulin/IGF signaling pathway (IIS) is a prominent regulator of aging of worms, flies, mice and likely humans. Delayed aging by IIS reduction protects the nematode, *C. elegans*, from toxicity associated with the aggregation of the Alzheimer's disease linked human peptide, Aβ. We reduced IGF signaling in Alzheimer's model mice and discovered that these animals are protected from the Alzheimer's-like disease symptoms including reduced behavioral impairment, neruoinflammation, neuronal and synpatic loss. This protection is correlated with the hyper-aggregation of Aβ leading to tightly packed, ordered plaques suggesting that one aspect of the protection conferred by reduced IGF signaling is the possible sequestration of soluble Aβ oligomers into dense aggregates of lower toxicity. These findings indicate that the IGF signaling regulated mechanism that protects from Aβ toxicity is conserved from worms to mammals and point to the modulation of this signaling pathway as a promising strategy for the development of Alzheimer's disease therapy.

§To whom correspondence should be addressed: dillin@salk.edu.
*Current address: Department of Biochemistry and Molecular Biology, the Institute for Medical Research Israel-Canada, The Hebrew University Medical School, Ein Kerem, Jerusalem, Israel.

Author contributions: EC and AD designed and initiated this study. EC crossed the mouse strains and performed the behavioral assays, the qPCR, ELISA, size exclusion and WB experiments. TBC performed IHC assays. Immuno-EM was carried out by JFP. DD executed *in-vitro* kinetic aggregation assays. PB performed image processing of the EM data. AA assisted with IHC. GE assisted with mice genotyping and behavioral assays. HMP assisted with WB. MH provided *Igf1r*+/− mice and expertise pertinent to *Igf1r*. EC, AD, JWK and EM wrote the manuscript.

Introduction

Most cases of Alzheimer's disease (AD) exhibit sporadic onset during the seventh decade of life or later, while the minority of cases are mutation-linked, familial disorders that typically manifest during the fifth decade. These temporal features, common to numerous neurodegenerative diseases, define aging as the major risk factor for the development of these maladies (Amaducci and Tesco, 1994). The insulin/insulin-like growth factor (IGF-1) signaling (IIS) pathway regulates stress resistance, aging and is a lifespan determinant. IIS reduction results in stress resistant, long-lived worms (Kenyon et al., 1993), flies (Tatar et al., 2001) and mice (Bluher et al., 2003; Holzenberger et al., 2003; Taguchi et al., 2007) and correlates with increased longevity of humans (Flachsbart et al., 2009; Suh et al., 2008; Willcox et al., 2008). Delayed aging, by IIS reduction, protects worms from proteotoxicity associated with the aggregation of the Huntington's disease associated polyQ peptide (Morley et al., 2002) and the AD-linked human Aβ peptide (Cohen et al., 2006). However, little is known about whether the protection from toxic protein aggregation provided by reduced IIS is conserved from worms to mammals, and what protective mechanisms may be operating.

Aβ originates from the endo-proteolysis of the Amyloid Precursor Protein (APP) (Glenner and Wong, 1984; Selkoe, 2004). The serine protease BACE (Beta Amyloid Cleaving Enzyme) cleaves APP (Farzan et al., 2000), followed by an intra-membrane cleavage of the resulting fragment by presenilin1 (PS1), an active component of the γ-secretase proteolytic complex (Wolfe et al., 1999). These events release a family of aggregation-prone peptides termed Aβ, including $A_{1–40}$ and the highly amyloidogenic $A_{1–42}$. Although compelling data indicate that Aβ aggregation triggers AD, the mechanism leading to the development of the disease remains unclear (Bossy-Wetzel et al., 2004; Selkoe, 2004). Recent studies hypothesize that it is not the high molecular weight fibrils, but small oligomeric Aβ species that lead to toxicity in AD model organisms (Cohen et al., 2006; Lesne et al., 2006) and to AD in humans (Caughey and Lansbury, 2003; Haass and Selkoe, 2007; Shankar et al., 2008) and while intriguing, this hypothesis warrants further scrutiny.

In the C. *elegans* Aβ model (Aβ worms, (Link, 1995)), the protection from human $Aβ_{1–42}$ proteotoxicity conferred by IIS reduction is dependent upon two transcription factors, Heat Shock Factor 1 (HSF-1), which regulates Aβ disaggregation, and DAF-16 (orthologue to FOXO in mammals) which facilitates the formation of larger, less toxic Aβ aggregates (Cohen et al., 2006). Accordingly, Aβ worms with reduced IIS that were protected from Aβ toxicity accumulated more large Aβ aggregates and had less oligomers compared to their unprotected counterparts exhibiting normal IIS (Cohen et al., 2006).

Although reduced IGF signaling extends the lifespan of mice (Bluher et al., 2003; Holzenberger et al., 2003; Taguchi and White, 2008), IGF-1 infusion protects from Aβ toxicity (Carro et al., 2002; Carro et al., 2006), raising the query of whether IGF signaling reduction or activation protects from Aβ toxicity (Gasparini and Xu, 2003). To address this question, we created an AD mouse model with reduced IGF signaling by crossing a well established AD transgenic mouse model (Jankowsky et al., 2001) with long-lived mice harboring only one *Igf1r* gene copy (*Igf1r*+/− mice) (Holzenberger et al., 2003).

Results

Creation of mice with AD transgenes in the context of reduced IGF-1R signaling

Igf1r is the mammalian orthologue of the sole worm insulin/IGF receptor *daf-2* (Kimura et al., 1997). *Igf1r*+/− mice have reduced signaling downstream of the IGF1 receptor, are long-

lived, oxidative stress resistant and have reduced body size (Holzenberger et al., 2003). The AD mouse model expresses two AD-linked mutated transgenes, APP_{swe} (a humanized mouse APP that contains the human Aβ peptide sequence) and human presenilin-1 ΔE9, both driven by the mouse prion protein promoter (hereafter referred to as *AD* mice) (Jankowsky et al., 2001). The expression of these transgenes results in the production of human Aβ, amyloid plaque formation in the brain and slow, progressive, age onset AD-like symptoms (Jankowsky et al., 2004). The *AD*-like mice also exhibit age onset behavioral impairments, analogous to other AD murine models (Reiserer et al., 2007). The *AD* model is not as aggressive as other AD models, exhibiting appearance of Aβ plaques in the brain at 6–7 months of age (Jankowsky et al., 2004). The relatively slow onset of AD-like symptoms in this model allows for the perturbation of IIS to examine its role in the age onset requirements of the AD-like syndrome.

To equalize the genetic background of our mice, we first backcrossed both the *AD* and *Igf1r* +/− mouse strains with wild-type 129 females (strain 129xi) for three generations, followed by four intercrosses between the *AD* and *Igf1r*+/− mice. Crossing *Igf1r*+/− with the *AD* mice generated offspring of four genotypes (Fig. 1A): The original parental genotypes; (i) heterozygous *Igf1r*+/− (***Igfr***+/−) and (ii) *AD* mice, which served as internal controls (***AD***). (iii) Congenic siblings that age naturally due to two *Igf1r* gene copies but carrying neither of the AD transgenes. These animals served as negative internal baseline controls for asymptomatic AD-like disease and natural IGF-1 signaling and were designated wild-type (**WT**). Finally, (iv) mice harboring both AD transgenes and only one *Igf1r* gene copy, serving as the experimental group of focus (***AD;Igf1r***+/−).

Quantitative PCR analysis revealed that the expression levels of the APP_{swe} transgene was nearly identical in brains of *AD* and *AD;Igf1r*+/− mice (Fig. S1, A–E), indicating that IGF signaling reduction does not effect the expression of the prion protein promoter driven transgenes. The levels of monomeric Aβ and of the C terminal APP fragment (APP CTF) were also very similar in *AD* and *AD;Igf1r*+/− mice (Fig. S1, F and G). We also tested whether reduced IGF signaling affected the levels of the endogenous murine α and β secretases (ADAM17 and BACE, respectively) utilizing western blot analysis, and found nearly identical levels of these proteins in brains of mice of all four genotypes (Fig. S1H). Together these results indicate that IGF signaling reduction affected neither the transgene expression nor the levels of the endogenous APP processing enzymes or their activity. As expected, both *Igf1r*+/− and the *AD;Igf1r*+/− mice were smaller in size in comparison to their littermates carrying two *Igf1r* copies, indicating reduced IGF-1R signaling (Fig. S2A (Holzenberger et al., 2003)).

Reduced IGF-1R signaling reduces the behavioral deficits of AD mice

Age onset memory deficiency, impairment of orientation, and locomotion are associated with Aβ production in numerous AD murine models (Jensen et al., 2005; King and Arendash, 2002; Westerman et al., 2002). To evaluate whether reduced IGF-1 signaling protects mice from behavioral impairments due to Aβ proteotoxicity, we used a battery of behavioral assays. As an initial analysis of age onset behavioral impairment, we utilized 8 animals per genotype and followed their performance in the Morris water maze test at 3, 6, 9 and 12 months of age to more narrowly define the time window in which the behavioral impairments became apparent. Analyzing the effect of the AD transgenes on the performance of the animals we found the greatest differences among *AD*, *AD;Igf1r*+/− animals and their littermate controls at the 9 and 12 month time points (Fig. S2, B and C). At 16 months we observed mortality in the *AD* group that was not present in the *AD;Igf1R*+/− mice (data not shown). Therefore, we refined our behavioral analysis to the 11–15 month time period using a larger cohort of animals.

We measured the learning ability of mice of the four genotypes using a Morris water maze with a cued (visible) platform for four consecutive days. As previously reported for other AD-model mouse strains (Blanchard et al., 2008; Westerman et al., 2002), the *AD* mice did not exhibit a learning deficiency compared to their age matched WT, *Igf1r*+/− and *AD;Igf1r* +/− counterparts (Fig. 1B, $P>0.05$). In contrast, the *AD* mice exhibited impaired orientation capabilities (Fig. 1C) (Jensen et al., 2005; King and Arendash, 2002; Westerman et al., 2002). In order to test orientation aptitude, we removed the cue from the platform and recorded the latency time required for mice of the four genotypes to locate the submerged platform for four consecutive days. At days 2, 3 and 4 of the experiment, *AD* mice required a significantly ($P<0.05$) longer time to find the hidden platform compared to their WT, *Igf1r* +/− and most importantly their *AD;Igf1r*+/− counterparts (Fig. 1C) (swim velocities were nearly identical for all genotypes (Fig. S2D)). Lastly, in order to test memory skills we removed the platform from the water maze and recorded the number of the crosses of the previous platform location (probe trial). *AD* mice crossed the previous location of the platform significantly ($P<0.05$) less times than their WT, *Igf1r*+/− and most importantly *AD;Igf1r*+/− counterparts, indicating impaired memory. In contrast, *AD;Igf1r*+/− animals crossed the previous platform location at similar frequencies compared to *WT* and *Igf1r*+/− animals suggesting partial memory restoration (Fig. 1D).

Next, we tested the effect of reduced IGF-1 signaling on the motor skills of AD model mice using a Rota-Rod assay. Much like the orientation and memory tests, *AD* mice performed significantly less well than their age matched WT, *Igf1r*+/− and *AD;Igf1r*+/− counterparts in the Rota-Rod assay (Fig. 1E, $P<0.05$).

Collectively, the behavioral data revealed that AD mice have impaired orientation and memory performance as well as locomotion impairment that can be delayed by the protection conferred by reduced IGF-1 signaling.

Reduced IGF-1R signaling reduces inflammation and neuronal loss in AD mice

We asked whether the appearance of biological markers associated with AD-like disease progression in mice was also delayed by reduced IGF-1R signaling. First we tested whether reactive astrocytosis, indicative of neuro-inflammation, associated with AD in humans (Mancardi et al., 1983) and with Aβ aggregation in the brains of AD-model mice (Wirths et al., 2008), was reduced in *AD;Igf1r*+/− animals. We utilized Glial Fibrilary Acidic Protein (GFAP) antibodies, which recognize activated astrocytes (Mancardi et al., 1983) and found notably less activated astrocytes in the brains of *AD;Igf1r*+/− mice compared to age matched *AD* mice (Fig. 2). This reduction was apparent both in the cortex and hippocampus (Fig. 2I), indicating that the neuro-inflammation associated with Aβ is largely reduced in *AD;Igf1r*+/− mice compared to age matched *AD* mice. Interestingly, while the GFAP signal observed in cortices of *AD* mice was largely diffuse, cortical GFAP staining of *AD;Igf1r*+/− mice appeared to be focal (compare Figs. 2C and D) suggesting that neuro-inflammation within *AD;Igf1r*+/− brains is confined to smaller areas compared to the brains of *AD* animals.

Neuronal loss is another hallmark of AD in humans (Scheff et al., 1990) and AD-model mice (Masliah and Rockenstein, 2000). We tested whether reduced IGF-1R signaling protects AD mice from this Aβ associated phenotype using direct stereological visualization and NeuN immunoreactivity, a marker of neuronal density that declines in *AD* mice. We found higher NeuN immunoreactivity in the cortices of 12–13 month old *AD;Igf1r*+/− mice compared to their age matched *AD* counterparts (Fig. 3), indicating that reduced IGF signaling protects from neuronal loss. Similar neuronal losses were observed in young (4–5 month of age) and in old (16–17 month) *AD* but not in *AD;Igf1r*+/− mice when compared to age matched control genotypes (Fig. S3).

Reduced synaptic density is an additional hallmark and probably causative of AD (Hamos et al., 1989). Thus, as a complementary approach, we compared synaptic densities in frontal and hippocampal brain regions of 12–13 month old mice of all genotypes using the synaptic marker synaptophysin (Dziewczapolski et al., 2009; Hamos et al., 1989). Our results indicate significantly lower synaptic densities in both frontal and hippocampal regions (Fig. 3J and 3K respectively) of *AD* animals compared to their *AD;Igf1r*+/− counterparts. These observations confirm that IGF signaling reduction protects mice form Aβ associated neuronal loss.

Reduced IGF signaling promotes the formation of densely packed aggregates

To explore the mechanism underlying the protection towards orientation, memory and locomotion deficiencies associated with reduced IGF signaling, as well as the protection from inflammation and neuronal and synaptic loss in mice ectopically expressing mutated AD-linked transgenes, we investigated the histological and biochemical nature of Aβ assemblies in brains of the unprotected *AD* and protected *AD;Igf1r*+/− mice. Immunohistochemistry (IHC) and Aβ antibodies (clone 6E10) were utilized to visualize Aβ plaques in brain sections from *AD* and *AD;Igf1r*+/− mice (Fig. S4). Consistent with previous results (Jankowsky et al., 2004), Aβ plaques could not be detected in brains of young mice (4–5 month old). A few plaques could be observed in the brains of 8–9 month old animals, whereas the number of plaques increased in the brains of 12–13 month old *AD* and *AD;Igf1r* +/− mice. No background staining was observed in brains of WT or *Igf1r*+/− mice at any age examined (Fig. S4). Therefore, reduced IGF-1R signaling has no apparent effect on the onset of plaque formation. To further analyze the Aβ plaque load we used the fluorescent dye Thioflavin-S to visualize amyloid within *AD* and of *AD;Igf1r*+/− brains. Our results (Fig. 4A) indicate that the amyloid load in *AD* and *AD;Igf1r*+/− mice were nearly identical in cortex and hippocampus (panel IX) (the plaque specificity of Thioflavin-S labeling was confirmed by the co-localization of Thioflavin-S signal with the signal of specific Aβ antibody (clone 82E1) (Fig S5A)). Therefore, the kinetics of appearance of Aβ plaques as well as the amyloid load did not appear to be a key difference between unprotected *AD* and protected *AD;Igf1r*+/− animals.

Closer inspection of the plaques analyzed by IHC revealed that Aβ plaques observed in the cortex of protected *AD;Igf1r*+/− animals appeared to be smaller in size and more condensed than plaques detected in the cortex of their age matched *AD* counterparts (Fig. S4, 12–13 month, insets). To compare the plaque compaction in the brains of *AD* and of *AD;Igf1r*+/− mice we used an additional, highly specific Aβ antibody (clone 82E1 that recognizes processed Aβ, residues 1–16) and measured the Aβ immunoreactive optical density (signal per area) in the different brains. We found significantly higher Aβ immunoreactive optical density in brains of *AD;Igf1r*+/− mice (Fig. 4B, panel IX), suggesting higher compaction of the Aβ amyloid plaques in these animals.

We compared the protease sensitivity of plaques of *AD* and *AD;Igf1r*+/− by treating brain sections of 12–13 month old mice with 10 μg/mL proteinase K prior to their labeling with Aβ antibody (clone 82E1). Although plaques of both genotypes were relatively resistant, we observed greater resistance of Aβ plaques of *AD;Igf1r*+/− animals as indicated by the diffuse staining of the plaques in *AD* brain slices compared to the protected *AD;Igf1r*+/− brain slices (Fig. S5B).

To further analyze the amyloid plaque density, we employed post-embedding immuno-electron microscopy using Aβ antibodies and gold-labeled secondary antibodies. Aβ fibrils in the cortex of *AD;Igf1r*+/− mice appeared to be more densely compacted than those of their *AD* counterparts (Figs. 5A and S6A) (the lack of immunoreactivity in the brain sections of WT and *Igf1r*+/− mice confirmed the specificity of the antibody staining (Fig. S6B)).

To quantify and compare the density of the amyloid plaques from *AD* and *AD;Igf1r*+/− mouse brains, we developed an image processing algorithm for the EM images. The algorithm identifies the gold particles conjugated to the Aβ antibodies (Fig. S6, C–F), sets a region of interest (ROI) around each gold particle and determines the median signal density within the ROI after excluding the gold particle (Fig. S6, G–I). ROIs that contain dense structures will have a lower score value due to less bright pixels and more dark pixels (i.e. lower gray scale value). Cortices of six 12–13 month old *AD* mice and five *AD;Igf1r*+/− mice were prepared for EM visualization and 135 images (34,087 ROIs) of *AD* and 101 images (26,066 ROIs) of *AD;Igf1r*+/− were automatically segmented and analyzed in an unbiased manner. The distributions of ROI median signal intensities indicate that plaques of *AD;Igf1r*+/− mice were significantly ($P<0.038$) more dense than age matched *AD* counterparts (Fig. 5B). The possibility that antibody accessibility differs among plaques of *AD* and *AD;Igf1r*+/− animals was assessed by a second algorithm which was designed to measure the distance between each gold particle and its closest neighboring particle. This algorithm is based of the assumption that lower accessibility would result in sparse distribution and longer distances among the gold particles. Automatic processing of all plaque images of *AD* and *AD;Igf1r*+/− (Fig. S6J) showed no difference in distances ($P>0.54$) indicating similar antibody accessibilities.

The results obtained using light and electron microscopy suggest that reduced IGF-1R signaling mediates the assembly of Aβ into more condensed amyloid plaques, reducing proteotoxicity. We used an *in-vitro* kinetic aggregation assay (Cohen et al., 2006) to assess the relative total amounts of Aβ amyloid in equal volumes of brains of *AD* and *AD;Igf1r*+/− mice. When proteinase K treated (degrades soluble proteins) and sonicated (fragments fibrils into a uniform size for quantification) brain homogenate is added to an $A\beta_{1-40}$ aggregation reaction in a test tube, the reduction in the time that it takes the aggregation reaction to reach 50% completion is proportional to the amount of Aβ amyloid fibrils in the tissue ((Cohen et al., 2006) and Deguo Du and Jeffrey Kelly, unpublished data). The amyloid load was assessed in 4–5 month and of 12–13 month old *AD* and *AD;Igf1r*+/− mouse brain homogenates (nine animals per genotype). While no significant difference in aggregate load could be detected amongst brain homogenates of young animals (4–5 months old, Fig. S6K), brain extracts of 12–13 month old *AD;Igf1r*+/− mice exhibit a higher aggregate load reflected by a shorter t_{50}, suggesting accelerated aggregation of $A\beta_{-40}$ in *AD;Igf1r*+/− relative to age matched *AD* animals (Fig. 5C; $P=0.035$). These data demonstrate that there is more amyloid in an equal volume of 12–13 month old *AD;Igf1r*+/− brain relative to *AD* brain. These results are consistent with the light and electron microscopy data indicating that protected *AD;Igf1r*+/− animals have more densely packed Aβ aggregates compared to unprotected *AD* animals. and thus it is consistent that there are more amyloid fibrils in a given brain volume.

Reduced IGF-1R signaling increases high MW aggregates and reduces SDS-soluble aggregates

The hyper-aggregation of Aβ by reduced IGF-1 signaling predicts lower residual amounts of non-aggregated Aβ and/or oligomeric Aβ. Therefore, we tested whether there was more soluble Aβ present in *AD* compared to *AD;Igf1r*+/− brain homogenates. We spun brain homogenates of 7 *AD* and 9 *AD;Igf1r*+/− 12–13 month old mice to sediment highly aggregated Aβ (10,000g for 10min, 4°C) and quantified the lower molecular weight $A\beta_{1-40}$ and $A\beta_{1-42}$ levels in the soluble fractions using ELISA assays. Our results indicate that $A\beta_{1-40}$ (Fig. 6A) and $A\beta_{1-42}$ (Fig. 6B) levels were significantly ($P<0.001$ and $P<0.005$, respectively) lower in the soluble brain supernatant fractions of *AD;Igf1r*+/− mice compared to age matched (12–13 month) *AD* animals. No such differences could be detected in the

amounts of soluble $A\beta_{1-40}$ among young mice, which had yet to exhibit plaque formation (Fig. S7A, P=0.126).

Next, we tested whether SDS soluble Aβ oligomeric content and total quantities were affected by reduced IGF-1R signaling. Four AD and 4 *AD;Igf1r*+/− mouse brains of 12–13 month old mice were subjected to an Aβ oligomer preparation protocol (Bar-On et al., 2006; Gong et al., 2003) followed by SDS-PAGE visualized by Western Blot (WB). Surprisingly, the SDS soluble Aβ oligomer content, total quantities and amounts of APP were indistinguishable in the total brain homogenates (Fig. 6, C and D) of *AD* and of *AD;Igf1r*+/− mice (no oligomers could be detected in cytosolic fractions (Fig. S7B)). The difference between the oligomer analysis results and the marked difference in the pool of non-aggregated Aβ species among *AD;Igf1r*+/− and *AD* animals observed by the ELISA assays (Fig. 6, A and B) suggests that the oligomeric Aβ assemblies might be SDS sensitive. To test this possibility, we employed size exclusion chromatography (SEC) to analyze the native composition of Aβ assemblies in the brains of *AD* and *AD;Igf1r*+/− mice. Brains of *AD;Igf1r*+/− and *AD* mice were homogenized and prepared as done for the ELISA assays to preserve macromolecular structural integrity (10,000g, 10min, 4°C). Equal amounts of cleared homogenates (Fig 6E panel i) were loaded onto a Superdex 75 size exclusion column, 20 fractions were collected (1ml per fraction), lyophilized, resuspended and loaded onto 4–12% Bis-Tris SDS gels. Aβ assemblies were visualized using WB and Aβ antibody (6E10). Notably, higher MW assemblies were observed in the *AD;Igf1r*+/− (see red reference line) reflecting that they were larger to begin with and/or that they were more SDS resistant (Fig. 6E, panel iii fraction 3) (for size exclusion standard see Fig. S7, C and D). The apparent dimer band resulting from SDS mediated denaturation of much larger aggregates previously linked to proteotoxicity is not observable in the *AD;Igf1r*+/− SEC fractions (Fig. 6E panel iii), but is observable in the *AD* mouse fractions, (Fig. 6E, panel ii fractions 5–7, open arrowhead), suggesting that in the *AD;Igf1r*+/− brains, Aβ fibrils are denser, more SDS resistant and more efficiently prevent the release of potentially toxic oligomeric species. Since toxicity has been previously associated with the capacity of high molecular weight assemblies to fragment (Shankar et al., 2008), prior correlations between the appearance of small SDS-stabilized Aβ species and neurotoxicity may reflect this. The data obtained from the microscopic analyses, ELISA and *in-vitro* assays suggest that the conversion of oligomers into denser, higher MW, more SDS-resistant aggregates is part of the process that protects against proteotoxicity in the *AD;Igf1r*+/− animals.

Discussion

By comparing behavioral and pathological aspects of Alzheimer's-like disease in the *AD* and *AD;Igf1r*+/− mice, we found that reduced IGF-1 signaling notably protects mice from proteotoxicity associated with the expression of the AD-linked human peptide, Aβ. Light and electron microscopy, as well as *in-vitro* kinetic aggregation, ELISA and size exclusion chromatography assays all indicate that reduced IGF-1 signaling induces the assembly of Aβ into a larger quantity of densely packed, larger fibrillar structures late in life. The observation that the protected *AD*;*Igf1r*+/− mice form SDS stable Aβ assemblies, making it more difficult to generate dimers previously linked to proteotoxicity (Shankar et al., 2008), suggests that an active mechanism may convert oligomers into densely packed aggregates of lower toxicity that protect the *AD*;*Igf1r*+/− mice from proteotoxicity. This hypothesis is consistent with results obtained in the Aβ worm model, where reduced insulin/IGF signaling protected worms from Aβ associated toxicity while increasing the formation of high molecular weight Aβ aggregates (Cohen et al., 2006).

How can increased Aβ aggregation protect against proteotoxicity? Highly aggregated Aβ is thought to bear lower toxicity in comparison to oligomers (Haass and Selkoe, 2007).

Accordingly, enhanced fibrillization is known to reduce Aβ toxicity in an AD-murine model (Cheng et al., 2007). Furthermore, results from long term potentiation (LTP) assays indicate that highly aggregated (plaque/fibrillar) Aβ bears lower toxicity than small oligomers (Shankar et al., 2008). Intriguingly, the release of small oligomers, most notably dimers, from large Aβ assemblies (fibrils) by chemical extraction increases toxicity. In support of the hypothesis that accelerated aggregation can be protective was provided by the discoveries that the cellular chaperones HSP104 (Shorter and Lindquist, 2004) and TRiC (Behrends et al., 2006), both known to disrupt toxic protein aggregates can also mediate protection by accelerating aggregation when the concentration of the aggregating protein exceeded a threshold level. These studies raise the prospect that the creation of densely packed, large Aβ assemblies protects *AD;Igf1r*+/− mice from proteotoxicity by trapping and storing highly toxic small aggregate structures in cooperation with the disaggregase activity. If active aggregation protects from Aβ toxicity, such protective mechanism might be expected to be negatively regulated by the IGF signaling pathway. In the worm, this activity is mediated, at least in part, by the FOXO transcription factor DAF-16 (Cohen et al., 2006) which is negatively regulated by the IIS receptor DAF-2. The FOXO gene family is highly conserved in mammals, is expressed in neurons and required for neuronal survival under stress (Lehtinen et al., 2006), suggesting that FOXO transcription factors are also mediators of the reduced IGF signaling protective effect in mammals.

It is likely that reduced IGF signaling ameliorates Aβ proteotoxicity by mechanisms in addition to Aβ dense fibril formation. The observation that *Igf1r*+/− mice exhibit increased resistance to oxidative stress (Holzenberger et al., 2003) raises the possibility that a reduction in IGF-1 signaling enhances the neuronal counter proteotoxic capabilities by enhancing the levels of enzymes that protect against oxidative stress that has been proposed to be involved in AD-associated brain damage (Fukui et al., 2007). This theme is supported by the observation that the production of reactive oxygen species (ROS) is reduced in brains of *Igf1r*+/− mice compared to their WT counterparts following 1-Methyl-4-phenyl 1-1,2,3,6-tetrahydropyridine (MPTP) treatment known to induce a Parkinson's Disease-like phenotype (Nadjar et al., 2008). Moreover, the over-expression of mitochondrial targeted catalase promotes longevity of mice (Schriner et al., 2005). An alternative model suggests that increased neuronal resilience associated with reduced IGF signaling is promoted by enhanced DNA repair capabilities. It is reasonable to speculate that the histone deacetylase SIRT1, an aging regulator (Ghosh, 2008) that plays roles in the maintenance of genomic stability (Oberdoerffer et al., 2008) and regulates HSF1 (Westerheide et al., 2009) may also be a mediator of the reduced IGF signaling protective effect in the *AD;Igf1r*+/− mice. The complexity and variety of effects mediated by FOXO (Partridge and Bruning, 2008) propose that reduced IGF signaling orchestrates an array of counter proteotoxic activities including Aβ hyper-aggregation, counter oxidation activities and presumably other yet to be defined mechanisms (Fig. 7). Further research is required to elucidate whether mammalian FOXO family members play roles in the reduced IGF mediated protective mechanism towards AD.

The Aβ hyper-aggregation observed in protected *AD;Igf1r*+/− mouse brains suggested that Aβ plaques would be visible in the cortex of these animals at younger ages compared to their unprotected AD counterparts, however, this was not evident in our analysis. This is likely due to other mechanisms of protein homeostasis being effective early in life, such as the disaggregase and degradation activity regulated by HSF-1, as observed in the worm (Cohen et al., 2006). A plethora of studies that link the heat shock response (Westerheide and Morimoto, 2005) and molecular chaperones (Muchowski and Wacker, 2005) to protection against neurodegenerative disorders reinforces this theme. In this view, the protective disaggregation/degradation and hyper-aggregation mechanisms may be temporally distinct. Active hyper-aggregation may only be invoked once the primary disaggregation machinery can no longer effectively clear toxic Aβ species as a consequence

of aging or an extrinsic stress. It will be interesting to evaluate whether one or more of the four HSF genes in the mouse are involved in protecting the brain from Aβ toxicity throughout life, and whether FOXO activity becomes prominent later in life.

There is an apparent contradiction between the data presented herein and earlier reports that IGF infusion protects rats (Carro et al., 2002) and mice (Carro et al., 2006) from Aβ associated proteotoxicity and that IGF-1R blockade induced neurological disease in rats (Carro et al., 2006). The presence of feedback signaling events that respond to the sudden increase in IGF concentration by tuning down the responsiveness of the IGF signaling cascade over time could explain why IGF infusion is protective against AD like pathology (Cohen and Dillin, 2008). This explanation is supported by many observations. For example, long-lived female human centenarians have high serum IGF-1 levels, but low IGF-1R activity - leading to reduced IGF signaling (Suh et al., 2008). Therefore, high IGF-1 levels do not necessarily correlate with increased downstream activity over a prolonged time. Additionally, AD patients have lower than normal serum insulin concentrations, but higher than normal CSF insulin levels (Craft et al., 1998). These studies raise the prospect that insulin and IGF signaling are regulated in a tissue specific manner and suggest that peripheral IGF infusion may lead to reduced IGF signaling in the brain (Cohen and Dillin, 2008).

The data presented here demonstrate that reduced IGF-1R signaling results in a profound reduction in the toxicity associated with Aβ expression in the brains of mice. The formation of more, larger and more dense Aβ aggregates that appear to be more SDS resistant in the *AD;Igf1r*+/− mice suggests that this is one core protective activity regulated at least in part by IGF-1R signaling, much like the disaggregase activity reported previously (Cohen et al., 2006) . The indication that reduced IIS is protective in nematodes and mammals stresses that manipulation of the highly conserved IGF signaling pathway, and its downstream components, is promising for the development of novel neurodegeneration and proteotoxicity therapies.

Experimental procedures

Mouse strains and genotyping

AD-model male mouse expressing a mutant chimeric mouse/human APP_{swe} and a mutant human presenilin 1 (Delta E9) both driven by the prion protein promoter was purchased from Jackson laboratory (Strain B6C3-Tg, (APP_{swe} PSEN1dE9) 85Dbo/J, Stock number 004462). Long-lived, compromised IIS mice: Males harboring only one *Igf1r* copy (S129 background, as described previously (Holzenberger et al., 2003)) were obtained from Dr. Jeffery S. Friedman (TSRI La Jolla, CA). Males of both strains were crossed for 3 generations with “wild-type” 129 females (Jackson laboratories, strain 129Xi/SvJ, Stock number 000691), to setup two separate colonies. Mice of each colony were backcrossed for additional two generations. Next, *Igf1r*+/− males were crossed with AD females for three generations to generate the experimental mice. Biopsies were taken form mouse tails at age 8–10 weeks and DNA was purified and subjected for PCR. APP_{swe}, and PS1ΔE9 were amplified according to Jackson laboratories instructions. *Igf1r* was amplified using the primers: forward: GTATAGTCCTAGAGGCCC reverse: GTTCTGGCAGAAAACATGG

Western Blot Analysis

From each case, brains were dissected, homogenized and divided by ultracentrifugation into cytosolic and membrane (particulate) fractions (Rockenstein et al., 2007). For Western blot analysis, 15 μg per lane of cytosolic and particulate fractions, assayed by the Lowry method, were loaded into 10% SDS-PAGE gels and blotted onto nitrocellulose paper. Briefly, as

previously described (Hashimoto et al., 2002), blots were incubated with antibodies against APP/Ab (6E10), Ab (82E1) and c-terminus APP (CT-15, courtesy of Dr. Ed Koo). After overnight incubation with primary antibodies, membranes were incubated with secondary antibodies tagged with horseradish peroxidase (HRP, 1:5000, SantaCruz Biotechnology, Inc., Santa Cruz, CA) and visualized by enhanced chemiluminescence and analyzed with a Versadoc XL imaging apparatus (BioRad, Hercules, CA). Analysis of actin levels was used as loading control.

Behavioral assays

Rota Rod

Locomotion was tested using Rota Rod system (EconoMex, Columbus instruments, Columbus, OH). Four mice were place at a time on the rotating beam set to accelerate at 0.2 rpm/sec. Time from start until each mouse fell off was recorded. Each mouse was trained one day for five times prior to the experiment. Each mouse was tested 5 times a day, four sequential days (total of 20 measurements/mouse/age). At least 12 animals (males and females) per genotype were used in each time point (supplemental statistical data).

Morris water maze

The Morris water maze was conducted as described previously (Jensen et al., 2005). Briefly, 11–15 old month old mice of the four genotypes were placed one animal per cage and numbered randomly to avoid genotype identification during the experiment. A white plastic tank 120 cm in diameter was filled with room temperature water (23°C), which was made opaque with white non-toxic Crayola paint. A transparent platform (8cm×12cm) was located in the center of one of the four virtually divided quadrants and was submerged 0.5cm below the water surface to be invisible. Distal cues, such as painted cardboard on the white wall, were provided in all experiments as spatial references. Mice were let swim until platform was found or for a maximum of 60 seconds. Mice were allowed to rest on the platform for 15sec between trials. In all experimental settings we utilized a video tracking system (Ethovision; Noldus Information Technology, Leesburg, VA) to record and analyze the swimming path, swim velocity, time taken to reach the platform (latency) and time spent in each quadrant. The experiments were performed at the following order: cued platform (four sequential days), one-day break, hidden platform (four sequential days), probe trial (one day). Number of animals used 13 (WT), 12 (*Igf1r*+/−), 8 (*AD*) and 15 (*AD;Igf1r*+/−).

Cued platform

For the cued version of water maze testing, the platform was located 0.5cm below the opaque water level but made clearly visible to the mouse by locating a 15cm high stick carrying a dotted flag (3cm×4cm) on the platform. The platform location was fixed throughout the experiment. The mice were released from four different locations around the water tank.

Hidden platform

The platform was located at the same location used for the cued platform experiment, 0.5cm below the opaque water level but without the dotted flag, to be invisible. The mice were released from four different locations around the tank. Time of latency, swim velocity, path length and time spent at each quadrant were recorded.

Probe trial

The platform was removed and the mice were allowed to swim for 40 seconds. The time spent in each quadrant and in the previous platform location, number of crossing the area were the platform was previously located, swim velocity and path length were recorded.

Size exclusion chromatography

A Superdex 75 10/300 GL column (Cat # 17-5174-01 GE Healthcare, Uppsala Sweden) attached to an AKTA FPLC system was used to separate Aβ oligomers from mouse brains. Column was calibrated using low molecular weight calibration kit (GE healthcare cat # 28-4038-41). 250μl of 10% (w/v) mouse brain homogenate (in PBS) was injected into the column and eluted with 50mM ammonium acetate, pH8.5 at flow rate of 0.5 ml/min. Twenty 1 ml fractions were collected, lyophilized, resuspended in 120μl PBS and 40μl LDS sample buffer, boiled for 10min and separated on 4–12% Bis-Tris gels as described above.

Morphological and post embedding immuno-electron microscopy

WT, *Igf1r*+/−, *AD* and *AD;Igf1r*+/− mice were sacrificed at the indicated ages. A piece of cortex from each mouse brain was immediately fixed for 24 hours in cold 2% paraformaldehyde and 0.25% glutaraldehyde in PBS (n=32; 2 animals from each genotype and time point). The tissue was washed in PBS and postfixed in 1% osmium tetroxide in PBS, washed in PBS and dehydrated in graded ethanol solutions followed by propylene oxide and embedded in Epon/Araldite mixture (Cat # 13940 Electron Microscopy Sciences, Hatfield, PA). The polymerized resin was sectioned (70nm) using a diamond knife (Diatome, Hatfield, PA). Sections were mounted on uncoated 400 mesh nickel grids (Cat# G400-Ni, Electron Microscopy Sciences) for immunolabeling. Antigen retrieval was performed by incubating samples in sodium m-periodate saturated aqueous solution for 10 minutes followed by Tris-Buffered Saline (TBS; 50 mmol/l Tris–HCl,150 mmol/l NaCl, pH 7.4) wash. Sections were background blocked in 3% bovine serum albumin (BSA) in TBS for 30 minutes followed by an over night incubation in primary $A\beta_{1–42}$ affinity purified polyclonal rabbit antibody which recognizes the C- terminus of the peptide (Cat # AB5078P Chemicon-Millipore, Temecula, CA (see for reference: (Takahashi et al., 2008)) 1:50 in 1% BSA in TBS at RT. Sections were washed 3 times in TBS and blocked in 3% BSA in TBS for 30 minutes followed by 2 hour incubation in protein A conjugated to 10nm gold particles (Cat # EM PAG10 BB International, Cardiff, UK) diluted 1:100 in 1% BSA in TBS at RT, rinsed 3 times in TBS, 3 times in H20 and air dried. Sections were contrasted with 2% uranyl acetate in 50% ethanol for 10 min and in Reynold's lead citrate solution (120 mmol/l sodium citrate, 25 mmol/l lead citrate, pH 12) for 1.5 minutes. The specimens were studied in a Jeol 100CX electron microscope (Jeol, Akishima, Tokyo, Japan) at 100 kV and electron micrographs were taken with a Mega View III CCD camera (Soft Imaging System GmbH, Muenster, Germany) linked to Analysis Pro v 3.2 digital micrograph software (Soft Imaging System GmbH).

In-vitro kinetic Aβ aggregation assay

$A\beta_{1–40}$ peptide was diluted to a final concentration of 10μM in phosphate buffer (300mM NaCl, 50mM Na-phosphate, pH 7.4) containing ThT (20μM). Mouse brain homogenate was sonicated for 40 min in a water bath sonicator (FS60, Fisher Scientific, Pittsburg, PA), treated for 2 hours with proteinase K (0.2μg/ml) and supplemented with complete EDTA-free protease inhibitor cocktail (cat#1836170 Roche, Basel Switzerland). The mixed solution was added to the assay at a final total protein concentration of 10μg/ml. Three aliquots (100μl) were transferred into wells of a 96-well microplate (Costar black, clear bottom) for each reaction. The plate was sealed and loaded into a Gemini SpectraMax EM fluorescence plate reader (Molecular Devices, Sunnyvale, CA), where it was incubated at 37°C. The fluorescence (excitation at 440nm, emission at 485nm) was measured from the bottom of the plate at 10 min intervals, with 5s of shaking before each reading. Half maximal fluorescence time points (t_{50}) were defined as the time point at which ThT fluorescence reached the middle between pre- and post-aggregation baselines. Fluorescence traces and t_{50} values represent averages of at least three independent experiments.

EM particle analysis

We have developed an unsupervised algorithm for automatic densitometry image analysis of gold-labeled electron-microscope images (see methods). The algorithm consists on two major steps: i) gold particle segmentation via adaptive thresholding and ii) gold particle removal prior to intensity measurment on a region of interest (ROI) located around each labeled particle. For the segmentation of gold particles, we use and adaptive threshold selection for each image. The first step of this algorithm consists on performing a survey of segmentation results for different thresholds. Then, based on this survey, a threshold is selected such that it results in high detection rate combined with negligible false-positive rate (Fig. S6C). For simplicity three segmentation regimes are shown at low threshold levels (th1 in Figs. S6C and D) no objects are segmented. As the threshold is increased objects start to be detected. Due to its three dimensional nature, the core of the gold-labeled particle has higher density at the center (thus a lower gray scale value). As such, object's median area increases with threshold, up to a point where some background pixels start to be included into the segmented results (but not contiguous to the labeled particles) at this point, the mean object area starts to decrease and the number of objects starts to rise (second regime). It is within this regime that the th2 threshold is selected (Fig. S6C). It is depicted in Fig. S6E that the adaptive threshold selection results in a satisfactory segmentation. Further increasing the threshold resulted in further decrease in object size and a fast increase in the number of segmented objects (third regime, th3 and its corresponding segmentation results (Fig. S6, C and F). Next, segmented object were filtered by their area, outliers where consider to be either smaller than the 2.5% or larger than the 97.5% quantiles or if having areas smaller than $9nm^2$ or larger than $180nn^2$; these values where obtained thorough inspection of the segmentation results on a small image dataset (n=10 images).

Plaque density is then estimated in a ROI of ~$500nm^2$ (41 × 41 pixels) centered around each of the segmented and area-filtered gold particles. To obtain an unbiased metric the gold particle is removed after estimating the appropriate threshold, here again this process is performed for each ROI separately. This threshold is estimated based on set of four intensity profiles obtained by sampling the image across its main diagonal and along the pixel lines that cross the center of the ROI (a single such image profile is shown in Fig S6G). Each intensity profile is processed to provide a single threshold estimate, then the median of these estimates is compute and further implemented. First the inverse of the profile is computed then thresholded at 0.05% of the maximal value. The purpose of this step is to provide a sharp boundary between pixels along the image profile that belong to the gold particle and the ones that do not. Next, starting from the center of the intensity profile, the left and right first positions that equal zero are selected and their value along the image profile serves as single threshold estimate. By doing so we avoided measuring other particles that might have been included in the current ROI. If such particles are present, they will also be removed when the median estimated threshold is applied to the ROI. Following gold particle removal, the total intensity is measured for the remaining pixels (`included' area in Fig S6I) and divided by its corresponding area, thus providing an estimate of placque density via its corresponding median gray level intensity. This algoritm was implemented in Matlab (Matworks Inc) and is available upon request (www.dillinlab.googlepages.com)

Supplementary Material

Refer to Web version on PubMed Central for supplementary material.

Acknowledgments

We thank Dr. Hyun-Eui Kim for expert assistance with size exclusion chromatography and Dr. Gustavo Dziewczapolski for expert assistance with behavioral assay.

This is study was generously supported by the McKnight Endowment for Neuroscience (AD) and NIA P01 AG031097 (AD, JWK, EM).

References

Amaducci L, Tesco G. Aging as a major risk for degenerative diseases of the central nervous system. Curr Opin Neurol 1994;7:283–286. [PubMed: 7952234]

Bar-On P, Rockenstein E, Adame A, Ho G, Hashimoto M, Masliah E. Effects of the cholesterol-lowering compound methyl-beta-cyclodextrin in models of alpha-synucleinopathy. Journal of neurochemistry 2006;98:1032–1045. [PubMed: 16895578]

Behrends C, Langer CA, Boteva R, Bottcher UM, Stemp MJ, Schaffar G, Rao BV, Giese A, Kretzschmar H, Siegers K, et al. Chaperonin TRiC promotes the assembly of polyQ expansion proteins into nontoxic oligomers. Molecular cell 2006;23:887–897. [PubMed: 16973440]

Blanchard J, Martel G, Guillou JL, Nogues X, Micheau J. Impairment of spatial memory consolidation in APP(751SL) mice results in cue-guided response. Neurobiology of aging 2008;29:1011–1021. [PubMed: 17350733]

Bluher M, Kahn BB, Kahn CR. Extended longevity in mice lacking the insulin receptor in adipose tissue. Science 2003;299:572–574. [PubMed: 12543978]

Bossy-Wetzel E, Schwarzenbacher R, Lipton SA. Molecular pathways to neurodegeneration. Nature medicine 2004;10(Suppl):S2–9.

Carro E, Trejo JL, Gomez-Isla T, LeRoith D, Torres-Aleman I. Serum insulin-like growth factor I regulates brain amyloid-beta levels. Nature medicine 2002;8:1390–1397.

Carro E, Trejo JL, Spuch C, Bohl D, Heard JM, Torres-Aleman I. Blockade of the insulin-like growth factor I receptor in the choroid plexus originates Alzheimer's-like neuropathology in rodents: new cues into the human disease? Neurobiology of aging 2006;27:1618–1631. [PubMed: 16274856]

Caughey B, Lansbury PT. Protofibrils, pores, fibrils, and neurodegeneration: separating the responsible protein aggregates from the innocent bystanders. Annu Rev Neurosci 2003;26:267–298. [PubMed: 12704221]

Cheng IH, Scearce-Levie K, Legleiter J, Palop JJ, Gerstein H, Bien-Ly N, Puolivali J, Lesne S, Ashe KH, Muchowski PJ, et al. Accelerating amyloid-beta fibrillization reduces oligomer levels and functional deficits in Alzheimer disease mouse models. The Journal of biological chemistry 2007;282:23818–23828. [PubMed: 17548355]

Cohen E, Bieschke J, Perciavalle RM, Kelly JW, Dillin A. Opposing activities protect against age-onset proteotoxicity. Science 2006;313:1604–1610. [PubMed: 16902091]

Cohen E, Dillin A. The insulin paradox: aging, proteotoxicity and neurodegeneration. Nat Rev Neurosci 2008;9:759–767. [PubMed: 18769445]

Craft S, Peskind E, Schwartz MW, Schellenberg GD, Raskind M, Porte D Jr. Cerebrospinal fluid and plasma insulin levels in Alzheimer's disease: relationship to severity of dementia and apolipoprotein E genotype. Neurology 1998;50:164–168. [PubMed: 9443474]

Dziewczapolski G, Glogowski CM, Masliah E, Heinemann SF. Deletion of the alpha 7 nicotinic acetylcholine receptor gene improves cognitive deficits and synaptic pathology in a mouse model of Alzheimer's disease. J Neurosci 2009;29:8805–8815. [PubMed: 19587288]

Farzan, M.; Schnitzler, CE.; Vasilieva, N.; Leung, D.; Choe, H. BACE2, a beta -secretase homolog, cleaves at the beta site and within the amyloid-beta region of the amyloid-beta precursor protein. Proceedings of the National Academy of Sciences of the United States of America; 2000. p. 9712-9717.

Flachsbart, F.; Caliebe, A.; Kleindorp, R.; Blanche, H.; von Eller-Eberstein, H.; Nikolaus, S.; Schreiber, S.; Nebel, A. Association of FOXO3A variation with human longevity confirmed in German centenarians. Proceedings of the National Academy of Sciences of the United States of America; 2009. p. 2700-2705.

Fukui H, Diaz F, Garcia S, Moraes CT. Cytochrome c oxidase deficiency in neurons decreases both oxidative stress and amyloid formation in a mouse model of Alzheimer's disease. Proc Natl Acad Sci U S A 2007;104:14163–14168. [PubMed: 17715058]

Gasparini L, Xu H. Potential roles of insulin and IGF-1 in Alzheimer's disease. Trends Neurosci 2003;26:404–406. [PubMed: 12900169]

Ghosh HS. The anti-aging, metabolism potential of SIRT1. Curr Opin Investig Drugs 2008;9:1095–1102.

Glenner GG, Wong CW. Alzheimer's disease: initial report of the purification and characterization of a novel cerebrovascular amyloid protein. Biochemical and biophysical research communications 1984;120:885–890. [PubMed: 6375662]

Gong, Y.; Chang, L.; Viola, KL.; Lacor, PN.; Lambert, MP.; Finch, CE.; Krafft, GA.; Klein, WL. Alzheimer's disease-affected brain: presence of oligomeric A beta ligands (ADDLs) suggests a molecular basis for reversible memory loss. Proceedings of the National Academy of Sciences of the United States of America; 2003. p. 10417-10422.

Haass C, Selkoe DJ. Soluble protein oligomers in neurodegeneration: lessons from the Alzheimer's amyloid beta-peptide. Nature reviews 2007;8:101–112.

Hamos JE, DeGennaro LJ, Drachman DA. Synaptic loss in Alzheimer's disease and other dementias. Neurology 1989;39:355–361. [PubMed: 2927643]

Hashimoto M, Sagara Y, Everall IP, Mallory M, Everson A, Langford D, Masliah E. Fibroblast growth factor 1 regulates signaling via the GSK3{beta} pathway: implications for neuroprotection. J Biol Chem 2002;277:32985–32991. [PubMed: 12095987]

Holzenberger M, Dupont J, Ducos B, Leneuve P, Geloen A, Even PC, Cervera P, Le Bouc Y. IGF-1 receptor regulates lifespan and resistance to oxidative stress in mice. Nature 2003;421:182–187. [PubMed: 12483226]

Jankowsky JL, Fadale DJ, Anderson J, Xu GM, Gonzales V, Jenkins NA, Copeland NG, Lee MK, Younkin LH, Wagner SL, et al. Mutant presenilins specifically elevate the levels of the 42 residue beta-amyloid peptide in vivo: evidence for augmentation of a 42-specific gamma secretase. Human molecular genetics 2004;13:159–170. [PubMed: 14645205]

Jankowsky JL, Slunt HH, Ratovitski T, Jenkins NA, Copeland NG, Borchelt DR. Co-expression of multiple transgenes in mouse CNS: a comparison of strategies. Biomolecular engineering 2001;17:157–165. [PubMed: 11337275]

Jensen MT, Mottin MD, Cracchiolo JR, Leighty RE, Arendash GW. Lifelong immunization with human beta-amyloid (1–42) protects Alzheimer's transgenic mice against cognitive impairment throughout aging. Neuroscience 2005;130:667–684. [PubMed: 15590151]

Kenyon C, Chang J, Gensch E, Rudner A, Tabtiang R. A C. elegans mutant that lives twice as long as wild type. Nature 1993;366:461–464. [PubMed: 8247153]

Kimura KD, Tissenbaum HA, Liu Y, Ruvkun G. daf-2, an insulin receptor-like gene that regulates longevity and diapause in Caenorhabditis elegans. Science 1997;277:942–946. [PubMed: 9252323]

King DL, Arendash GW. Behavioral characterization of the Tg2576 transgenic model of Alzheimer's disease through 19 months. Physiology & behavior 2002;75:627–642. [PubMed: 12020728]

Lehtinen MK, Yuan Z, Boag PR, Yang Y, Villen J, Becker EB, DiBacco S, de la Iglesia N, Gygi S, Blackwell TK, et al. A conserved MST-FOXO signaling pathway mediates oxidative-stress responses and extends life span. Cell 2006;125:987–1001. [PubMed: 16751106]

Lesne S, Koh MT, Kotilinek L, Kayed R, Glabe CG, Yang A, Gallagher M, Ashe KH. A specific amyloid-beta protein assembly in the brain impairs memory. Nature 2006;440:352–357. [PubMed: 16541076]

Link, C. Expression of human beta-amyloid peptide in transgenic Caenorhabditis elegans. Proceedings of the National Academy of Sciences of the United States of America; 1995. p. 9368-9372.

Mancardi GL, Liwnicz BH, Mandybur TI. Fibrous astrocytes in Alzheimer's disease and senile dementia of Alzheimer's type. Acta neuropathologica 1983;61:76–80. [PubMed: 6353837]

Masliah E, Rockenstein E. Genetically altered transgenic models of Alzheimer's disease. Journal of neural transmission 2000;59:175–183. [PubMed: 10961430]

Morley, JF.; Brignull, HR.; Weyers, JJ.; Morimoto, RI. The threshold for polyglutamine-expansion protein aggregation and cellular toxicity is dynamic and influenced by aging in Caenorhabditis elegans. Proceedings of the National Academy of Sciences of the United States of America; 2002. p. 10417-10422.

Muchowski PJ, Wacker JL. Modulation of neurodegeneration by molecular chaperones. Nat Rev Neurosci 2005;6:11–22. [PubMed: 15611723]

Nadjar A, Berton O, Guo S, Leneuve P, Dovero S, Diguet E, Tison F, Zhao B, Holzenberger M, Bezard E. IGF-1 signaling reduces neuro-inflammatory response and sensitivity of neurons to MPTP. Neurobiology of aging. 2008

Oberdoerffer P, Michan S, McVay M, Mostoslavsky R, Vann J, Park SK, Hartlerode A, Stegmuller J, Hafner A, Loerch P, et al. SIRT1 redistribution on chromatin promotes genomic stability but alters gene expression during aging. Cell 2008;135:907–918. [PubMed: 19041753]

Partridge L, Bruning JC. Forkhead transcription factors and ageing. Oncogene 2008;27:2351–2363. [PubMed: 18391977]

Reiserer RS, Harrison FE, Syverud DC, McDonald MP. Impaired spatial learning in the APPSwe + PSEN1DeltaE9 bigenic mouse model of Alzheimer's disease. Genes, brain, and behavior 2007;6:54–65.

Scheff SW, DeKosky ST, Price DA. Quantitative assessment of cortical synaptic density in Alzheimer's disease. Neurobiology of aging 1990;11:29–37. [PubMed: 2325814]

Schriner SE, Linford NJ, Martin GM, Treuting P, Ogburn CE, Emond M, Coskun PE, Ladiges W, Wolf N, Van Remmen H, et al. Extension of murine life span by overexpression of catalase targeted to mitochondria. Science 2005;308:1909–1911. New York, NY. [PubMed: 15879174]

Selkoe DJ. Alzheimer disease: mechanistic understanding predicts novel therapies. Ann Intern Med 2004;140:627–638. [PubMed: 15096334]

Shankar GM, Li S, Mehta TH, Garcia-Munoz A, Shepardson NE, Smith I, Brett FM, Farrell MA, Rowan MJ, Lemere CA, et al. Amyloid-beta protein dimers isolated directly from Alzheimer's brains impair synaptic plasticity and memory. Nature medicine. 2008

Shorter J, Lindquist S. Hsp104 catalyzes formation and elimination of self-replicating Sup35 prion conformers. Science 2004;304:1793–1797. [PubMed: 15155912]

Suh, Y.; Atzmon, G.; Cho, MO.; Hwang, D.; Liu, B.; Leahy, DJ.; Barzilai, N.; Cohen, P. Functionally significant insulin-like growth factor I receptor mutations in centenarians. Proceedings of the National Academy of Sciences of the United States of America; 2008. p. 3438-3442.

Taguchi A, Wartschow LM, White MF. Brain IRS2 signaling coordinates life span and nutrient homeostasis. Science 2007;317:369–372. [PubMed: 17641201]

Taguchi A, White MF. Insulin-like signaling, nutrient homeostasis, and life span. Annu Rev Physiol 2008;70:191–212. [PubMed: 17988211]

Takahashi RH, Capetillo-Zarate E, Lin MT, Milner TA, Gouras GK. Co-occurrence of Alzheimer's disease beta-amyloid and tau pathologies at synapses. Neurobiology of aging. 2008

Tatar M, Kopelman A, Epstein D, Tu MP, Yin CM, Garofalo RS. A mutant Drosophila insulin receptor homolog that extends life-span and impairs neuroendocrine function. Science 2001;292:107–110. [PubMed: 11292875]

Westerheide SD, Anckar J, Stevens SM Jr. Sistonen L, Morimoto RI. Stress-inducible regulation of heat shock factor 1 by the deacetylase SIRT1. Science 2009;323:1063–1066. New York, NY. [PubMed: 19229036]

Westerheide SD, Morimoto RI. Heat shock response modulators as therapeutic tools for diseases of protein conformation. The Journal of biological chemistry 2005;280:33097–33100. [PubMed: 16076838]

Westerman MA, Cooper-Blacketer D, Mariash A, Kotilinek L, Kawarabayashi T, Younkin LH, Carlson GA, Younkin SG, Ashe KH. The relationship between Abeta and memory in the Tg2576 mouse model of Alzheimer's disease. J Neurosci 2002;22:1858–1867. [PubMed: 11880515]

Willcox, BJ.; Donlon, TA.; He, Q.; Chen, R.; Grove, JS.; Yano, K.; Masaki, KH.; Willcox, DC.; Rodriguez, B.; Curb, JD. FOXO3A genotype is strongly associated with human longevity. Proceedings of the National Academy of Sciences of the United States of America; 2008. p. 13987-13992.

Wirths O, Breyhan H, Marcello A, Cotel MC, Bruck W, Bayer TA. Inflammatory changes are tightly associated with neurodegeneration in the brain and spinal cord of the APP/PS1KI mouse model of Alzheimer's disease. Neurobiology of aging. 2008

Wolfe MS, Xia W, Ostaszewski BL, Diehl TS, Kimberly WT, Selkoe DJ. Two transmembrane aspartates in presenilin-1 required for presenilin endoproteolysis and gamma-secretase activity. Nature 1999;398:513–517. [PubMed: 10206644]

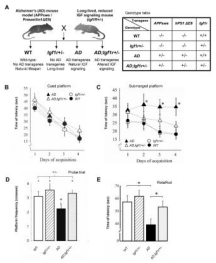

Figure 1.

Reduction of IGF signaling protects mice from Aβ associated behavioral impairments. **A.** Long-lived mice carrying one *Igf1r* copy were crossed with transgenic Alzheimer's disease (AD) model mice harboring two AD-linked mutated genes, APP_{swe} (containing the human Aβ sequence) and PS1ΔE9 to obtain offspring of four genotypes: (i) Wild Type – harbor two *Igf1r* copies and no AD linked transgenes (**WT**). (ii) Long-lived mice with one *Igf1r* copy and no AD linked transgenes (***Igf1r*+/−**). (iii) AD model mice with two *Igf1r* copies and both AD-linked transgenes (***AD***). (iv) Mice that harbor only one *Igf1r* copy and both AD-linked transgenes (***AD;Igf1r*+/−**). **B.** Latency time for reaching the cued platform significantly decreased through the acquisition sessions (*P*= 0, F = 35.49, df = 3) without differences between the four genotypes (*P*>0.05, F = 1.84, df = 3, n=8, 15, 16, 18 for *AD*, *AD;Igf1r*+/−, WT and *Igf1r*+/− respectively), suggesting no impairment of learning. **C.** For the submerged platform test significant differences were observed between genotypes (*P* = 5E-4, 2-Way-ANOVA, F=7.71, df = 3,) and across the acquisition days (*P* = 0.032, F = 2.97, df = 3, n=8, 15, 16, 18 for *AD*, *AD;Igf1r*+/−, WT and *Igf1r*+/−, respectively). The *AD* mice spent a longer time (*P*<0.05. Fisher-LSD) after the second day in order to find the submerged platform while no difference was observed among the three other genotypes. **D.** Analysis of the number of crosses of the previous platform location indicated that *AD;Igf1r* +/− animals crossed significantly (P=0.024, Kruskal-Wallis, χ^2 =9.38, df = 3) more times than their *AD* counterparts. **E.** We analyzed the performance of individuals after the age of plaque formation (i.e. 12–16 month) in a Rota Rod task. Animals of the different genotypes significantly differed in their performance (*P* < 0.01, one-way ANOVA, df = 3, F = 4.25; n = 31, 32, 29 and 28 individuals for *AD*, *AD;Igfr*+/−, *Igf1r*+/− and wild type, respectively). *AD* mice performed worst among the four genotypes while *AD;Igfr*+/− mice where partially rescued from this impairment as they performed significantly better than *AD* animals (p < 0.05, Tuckey's LSD). Yet no statistical difference appeared between this later genotype and the two other control genotypes. In all behavioral tests, 11–15 month old mice were tested and age match controlled.

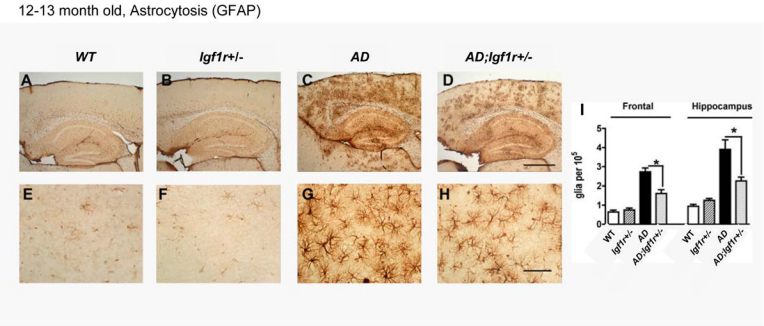

Figure 2.

Reduced IGF signaling reduces Aβ associated neuroinflamation. **A – H.** Immuno histochemistry using GFAP antibody indicated reduced astrocytosis in brain sections of 12–13 month old *AD;Igf1r*+/− mice (D and H) compared to age matched *AD* mice (C and G). **I.** Image analysis confirmed the significance of the GFAP signal difference (six mice per genotype and 3 sections per animal were analyzed, $P<0.05$).

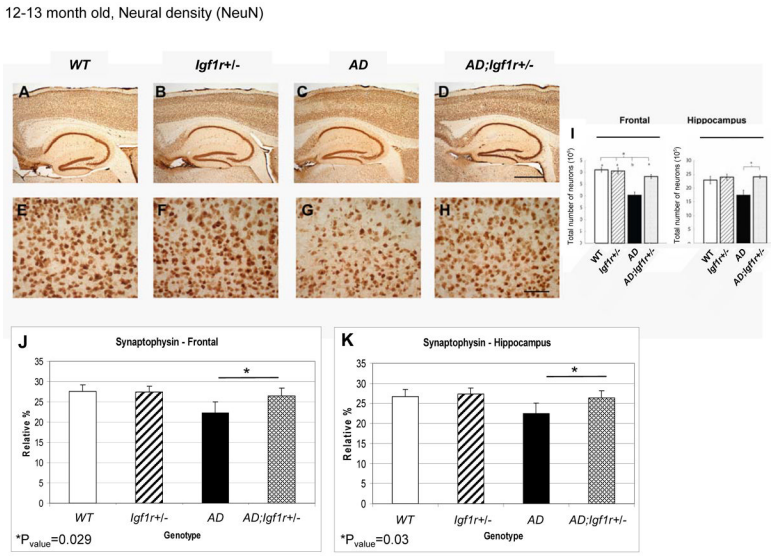

Figure 3.

Reduced IGF signaling protects from Aβ associated neuronal and synpatic loss. **A**–**H**. Immuno histochemistry using NeuN antibody indicated that neural densities in the brains of 12–13 month old *AD;Igf1r*+/− (D and H), WT (A and E) and *Igf1r*+/− (B and F) mice were comparable, while remarkable neuronal loss was observed in brains of age matched *AD* animals (C and G). **I.** Image analysis of the NeuN signals indicated that neural density in both cortices and hippocampuses of *AD* animals was significantly lower compared to their age matched WT counterparts (Cortex: $p<0.001$, One way ANOVA, $F=16.03$; Hippocampus $p<0.05$, Kruskal-Wallis $\chi^2=9.36$, $df=3$). No significant difference was observed among brains of *AD;Igf1r*+/− and *Igf1r*+/− mice (six mice per genotype and 3 sections per animal were analyzed). **J** and **K**. Immuno histochemistry using synaptophysin antibody revealed that *AD;Igf1r*+/− mice exhibit significantly higher synaptic densities than their age matched *AD* counterparts in both frontal (J) and hippocampal (K) brain regions (*AD* n=7, *AD;Igf1r*+/− n=5).

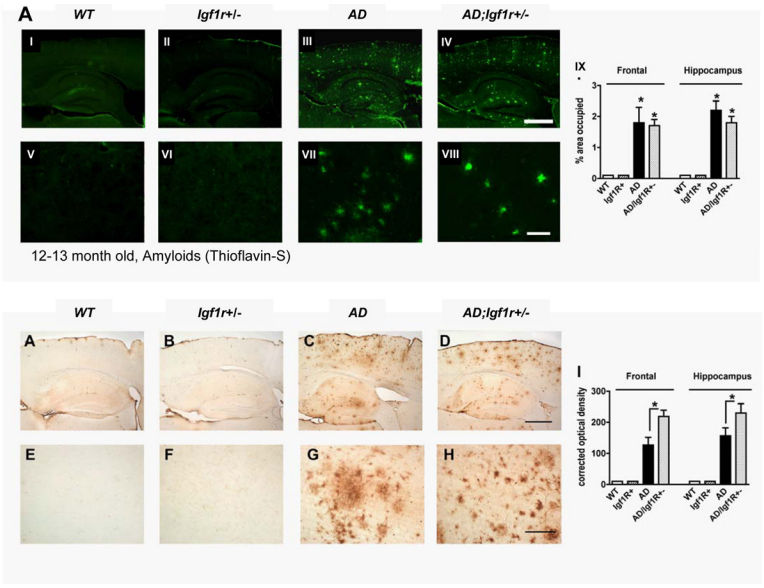

Figure 4.

Reduced IGF signaling facilitates Aβ hyper-aggregation. **A.** Thioflavin-S amyloid labeling showed similar Aβ plaque burden in brains of *AD* (panels III and VII) and *AD;Igf1r*+/− animals (panels IV and VIII). Image analysis indicated that the Thioflavin-S signals are similar in brains of *AD* and *AD;Igf1r*+/− mice, but signifcantly different from WT and *Igf1r* +/− mice (panel IX). Six 12–13 month old animals per genotype were analyzed. **B.** Aβ plaque signal density was measured using Aβ specific antibody (82E1). The signal per area ratio in brains of *AD;Igf1r*+/− animals (panels IV and VIII) was significantly higher (panel IX, $P<0.05$) compared to brains of age matched *AD* animals (panels III and VII) indicating higher plaque compaction in brains of *AD;Igf1r*+/− mice (six mice per genotype and 3 sections per animal were analyzed, DG – Dentate gyrus, NC – Neocortex).

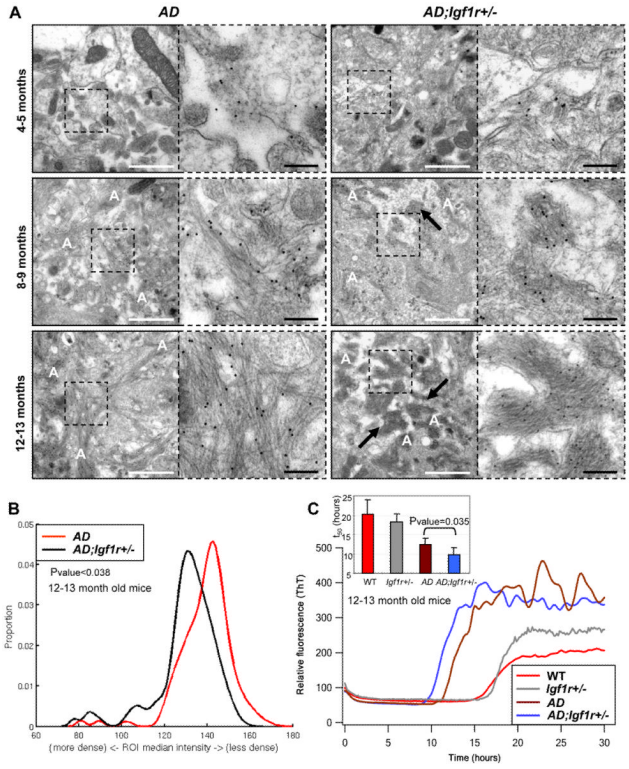

Figure 5.

Eleectron microscopy and *in-vitro* kinetic aggreagtion assays reveal densely packed Aβ aggregates in the brains of protected *AD;Igf1r*+/− *mice*. **A.** Electron micrographs of immuno-gold labelled Aβ amyloids in the cortex of *AD* and *AD;Igf1r*+/− mouse brains at different ages. Gold labeled amyloid and fibrillar Aβ structures can be observed in the higher magnification electron micrographs (right panels). The amyloid load similarly increased with age in both genotypes, but a highly ordered and condensed amyloid was present in *AD;Igf1r*+/− cortices (arrows) but not in the cortices of their *AD* counterparts (White scale bars 1 μm, black bars represent 200nm). **B.** Unbiased automated image processing indicates that median intensities of regions of interest (ROIs) around the gold particles labeling Aβ plaques of *AD;Igf1r*+/− mice (black) are significantly *(P*<0.04) lower than the plaque intensities of age matched *AD* animals (red), confirming the higher compaction state of Aβ plaques of *AD;Igf1r*+/− (six mice per genotype were processed, 135 images (34,087 ROIs) of *AD* and 101 images (26,066 ROIs) of *AD;Igf1r*+/− were collected and analyzed). **C**. Using an *in-vitro* kinetic aggreagtion assay to assess fibril load, 12–13 month old *AD;Igf1r*+/− mouse brain homogenates (blue) accelerated Thioflavin-T (ThT) monitored *in-vitro* kinetic aggregation significantly (*P*=0.035) faster than homogenates of age matched *AD* brains (brown) indicating more Aβ seeding competent assemblies in *AD;Igf1r*+/− mouse brains. **Inset:** statistical analysis of results obtained in C.

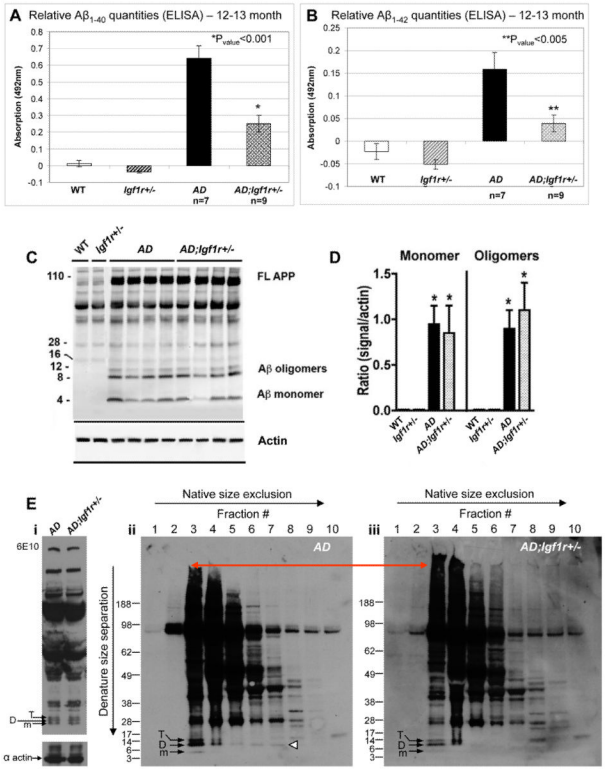

Figure 6.

AD brains contain more soluble Aβ oligomers than brains of *AD;Igf1r*+/− animals. **A and B.** ELISA assay detected significantly higher amounts of soluble $A\beta_{1–40}$ (A) ($P<0.001$) and $A\beta_{1–42}$ (B) ($P<0.005$) in brain homogenates of 12–13 month old *AD* mice compared to brains of age matched *AD;Igf1r*+/− animals. **C and D.** Western blot analysis reveals no detectable difference in the amount of SDS sensitive Aβ monomers and small oligomeric assemblies between *AD* and *AD;Igf1r*+/− brain homogenates. * indicates significant difference from WT or *Igfr1*+/− mice. **E**. Native size exclusion chromatography (SEC) indicated that Aβ dimers were mainly associated with large structures in brains of 16–17 month *AD;Igf1r*+/− mice (panel iii) while more soluble in brains of age matched *AD* animals (panel ii, arrowhead)(panels represent 6 *AD* and 6 *AD;Igf1r*+/− animals that were analyzed). Loading of total samples onto the gel and subsequent western blot analysis using 6E10, confirmed equal protein loading onto the column (panel i).

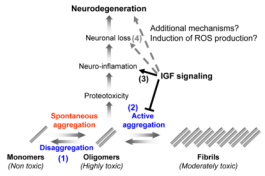

Figure 7.

IGF-1 signaling can play several roles in mitigating the toxicity of Aβ. The digestion of APP creates Aβ monomers that spontaneously aggregate to form toxic oligomers and possibly higher order structures in-vivo. At least two biological mechanisms can detoxifiy Aβ oligomers: (1) conversion of toxic oligomers into monomers (disaggregation) and (2) the conversion of the toxic oligomers into a much less toxic, larger structures (active aggregation). Within scenario 1, IGF-1 signaling could normally funciton to reduce protein disaggregases, possibly mediated by HSF transcription factors. Therefore, reduction of IGF-1 signaling would be predicted to result in less oligomers and more monomeric forms of Aβ due to the activation of protein disaggregases. Our resutls are inconsistent with this scenario since we find less oligomers, but equal amounts of monomeric forms of Aβ. Alternatively, within in scenario 2, IGF-1 signaling could normally function to reduce protective protein aggregases that convert toxic species into larger, less toxic forms. Therefore, reduced IGF-1 signaling results in increased aggreagase activity that in turn reduces the load of toxic oligomers and increases the compaction of less toxic fibrils. In support of scenario 2, we observed less soluble oligomers and higher compaction of the amyloid plaques in the AD animals with reduced IGF1R signaling (*AD;Igf1r*+/− animals). Alternatively, (3) IGF-1 signaling could promote protoeotoxicity and neuro-inflamation in response to toxic Aβ assemblies. Our results are also consistent with this proposed mechanism as we observed much less neuro-inflammation in the brains of protected *AD;Igf1r*+/− animals. However, this lower inflammation rate could be directly related to the reduction of Aβ oligomers in the protected animals by increased aggregases. Finally,in scenario 4, reduction of toxic secondary factors, such as Reactive Oxygen Species (ROS), might synergize with the production of toxic Aβ assemblies to promote neuronal loss. Consistent with this mechanism, *Igf1r*+/− mice are much more resistant to oxidative damage than wild type mice. Taken together, IGF-1 signaling could impinge at multiple steps on the path to neuronal loss and neurodegeneration in response to Aβ production and none of the interventions are mutually exclusive. Therefore, methods to reduced IGF-1 signaling provide multiple opportunities for disease intervention. Our data is most consistent with a model in which reduced IGF-1 signaling reduces the load of toxic Aβ structures, presumably dimers, that results in higher compaction of plaques, reduced neruo-inflammation and reduced neuronal loss.